

Performance of Particle Flow Calorimetry at CLIC

J. S. Marshall^a, A. Münnich^b, M. A. Thomson^a

^a*Cavendish Laboratory, University of Cambridge, Cambridge, United Kingdom*
^b*CERN, Geneva, Switzerland*

Abstract

The particle flow approach to calorimetry can provide unprecedented jet energy resolution at a future high energy collider, such as the International Linear Collider (ILC). However, the use of particle flow calorimetry at the proposed multi-TeV Compact Linear Collider (CLIC) poses a number of significant new challenges. At higher jet energies, detector occupancies increase, and it becomes increasingly difficult to resolve energy deposits from individual particles. The experimental conditions at CLIC are also significantly more challenging than those at previous electron-positron colliders, with increased levels of beam-induced backgrounds combined with a bunch spacing of only 0.5 ns. This paper describes the modifications made to the PandoraPFA particle flow algorithm to improve the jet energy reconstruction for jet energies above 250 GeV. It then introduces a combination of timing and p_T cuts that can be applied to reconstructed particles in order to significantly reduce the background. A systematic study is performed to understand the dependence of the jet energy resolution on the jet energy and angle, and the physics performance is assessed via a study of the energy and mass resolution of W and Z particles in the presence of background at CLIC. Finally, the missing transverse momentum resolution is presented, and the fake missing momentum is quantified. The results presented in this paper demonstrate that high granularity particle flow calorimetry leads to a robust and high resolution reconstruction of jet energies and di-jet masses at CLIC.

Keywords: Particle flow calorimetry, CLIC, Linear Collider

1. Introduction

CLIC [1] is a proposed linear collider designed to perform electron-positron collisions at centre-of-mass energies ranging from a few hundred GeV up to 3 TeV, with a luminosity of $5.9 \cdot 10^{34} \text{ cm}^{-2} \text{ s}^{-1}$ at the highest energy. The anticipated physics potential of such a collider is extremely broad. It ranges from precision tests of the Higgs and top sector, to detailed studies of new phenomena, through new particle spectroscopy, coupling measurements, threshold scans, measurement of spins and other quantum numbers. Accurate jet energy reconstruction will be crucial for this physics programme, driving the need for fine-grained calorimeters and the particle flow approach to calorimetry at CLIC.

This paper describes the performance of high granularity particle flow calorimetry at high energies and with the challenging background conditions present at CLIC. These studies build on those first reported in the context of the ILC [2]. The results presented here are based on full GEANT4 simulations of the CLIC_ILD [3] detector concept considered in the CLIC conceptual design report [1]. Results for the CLIC_SiD [4] detector concept

were comparable [5].

2. The Particle Flow Concept

Many of the interesting physics processes at CLIC will produce final states containing multiple jets, which may be accompanied by charged leptons and/or missing transverse momentum. In order to perform precision physics measurements, it is vital to be able to reconstruct the invariant masses of the jets; accurate jet mass measurements are a powerful tool for both reconstruction and identification of physics events. The goal for jet energy resolution at CLIC is that it should be sufficient to allow separation of the hadronic decays of W and Z bosons through the reconstruction of their di-jet invariant masses. This sets a challenging jet energy resolution goal of $\sigma_E/E \lesssim 5 - 3.5\%$ for 50 GeV – 1 TeV jets, which is unlikely to be achievable with a traditional approach to calorimetry [2].

Measurements of jet fragmentation at LEP provide detailed information about the particle composition of jets [6, 7]. In a typical jet, approximately 62% of the

energy is carried by charged particles (mainly hadrons), whilst 27 % is carried by photons, 10 % by long-lived neutral hadrons and 1.5 % by neutrinos. In a traditional approach to calorimetry, the jet energy would be obtained from the energies deposited in the electromagnetic and hadronic calorimeters (ECAL and HCAL respectively). This means that 72 % of the energy of a typical jet would be measured with a precision limited by the relatively poor HCAL resolution of $\gtrsim 55\% / \sqrt{E/\text{GeV}}$.

The particle flow approach to calorimetry aims to improve jet energy measurements by reconstructing the four-vectors of all visible particles in an event. The reconstructed jet energy is then the sum of the energies of the individual particles in the jet. At LEP, ALEPH used particle flow techniques [8] to improve the energy resolution for hadronic events. However, due to the relatively low granularity of the calorimeters, energy depositions from neutral hadrons still had to be identified as significant excesses of calorimetric energy compared to the associated charged particle tracks. Particle flow techniques are also being used by CMS [9] at the LHC.

The linear collider detector concepts extend the particle flow approach by using fine-granularity calorimeters and sophisticated software algorithms to accurately trace the individual paths of particles through the detector. The energy and momentum for each particle can then be determined from the detector subsystem in which the measurements are the most accurate. Charged particle momenta are measured in the inner detector tracker, whilst photon energy measurements are extracted from the energy deposited in the ECAL, with typical resolution $< 20\% / \sqrt{E/\text{GeV}}$. The HCAL is used to measure only the 10 % of jet energy carried by long-lived neutral hadrons. Particle flow calorimetry can therefore offer a significant improvement to jet energy measurements, compared to traditional calorimetry. For jet energies above about 100 GeV, the jet energy resolution is limited by the mistakes in the assignment of the energies to the different reconstructed particles, termed *confusion*, rather than the intrinsic resolution of the calorimeters.

3. Particle Flow Implementation

Figure 1 shows the typical topology of a simulated 250 GeV jet in the CLIC_ILD detector concept, with labels identifying a number of the constituent particles. The Figure shows inner detector tracks, representing the paths of charged particles in the Time Projection Chamber (TPC). These tracks can be extrapolated by eye and associated with clusters of calorimeter energy

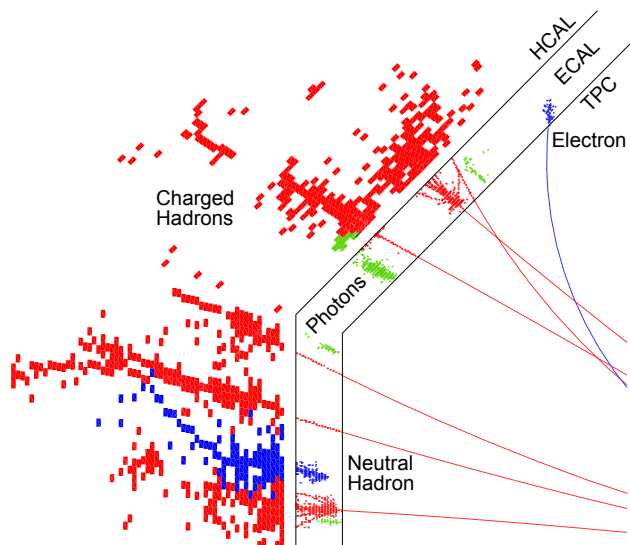


Figure 1: A typical simulated 250 GeV jet in CLIC_ILD, with labels identifying constituent particles.

deposits in the fine granularity ECAL and HCAL. Photons produce energy deposits with characteristic longitudinal and transverse profiles in the ECAL and can be cleanly resolved by eye, due to their small transverse spread. HCAL clusters that cannot be associated with TPC tracks represent neutral hadrons. The challenge is to develop software algorithms to automate the reconstruction of the individual particles from the tracks and energy deposits in the calorimeters.

Particle flow calorimetry demands high performance software. The final jet energy resolution is strongly dependent on both the detector granularity and the quality of the particle flow reconstruction algorithms. These algorithms must be able to exploit the granularity to merge together energy deposits from individual particles, with minimal confusion. A logical approach is to implement a series of decoupled pattern-recognition algorithms, each designed to carefully reconstruct a specific particle topology. The implementation of a large number of efficient pattern-recognition algorithms drives the need for a central software framework, which can take care of memory-management and book-keeping issues. Such a framework helps to keep each algorithm simple and focused on its specific pattern-recognition task.

The PandoraPFA C++ Software Development Kit (SDK) [10] for particle flow calorimetry is a robust and efficient framework for developing and running algorithms for particle flow reconstruction. It consists of a single framework library and a number of carefully

designed Application Programming Interfaces (APIs). It was designed with the twin aims of simplifying the development of efficient pattern-recognition algorithms and allowing easy application of existing algorithms to different detectors, different software environments or even different pattern-recognition tasks. Using the PandoraPFA SDK means that the pattern-recognition reconstruction is divided into three distinct sections, which communicate via the PandoraPFA APIs.

A PandoraPFA client application uses the APIs to pass details of the tracks and calorimeter cells in an event to the PandoraPFA framework. The framework then creates and manages its own lists of self-describing PandoraPFA tracks and cells. These objects are then accessed, in a controlled manner, by the PandoraPFA algorithms. The algorithms control the pattern-recognition reconstruction and determine how the tracks and cells are used to build clusters and, finally, reconstructed particles (termed particle flow objects, or PFOs). Importantly, the algorithms can only access or manipulate the PandoraPFA objects by using APIs to request services from the framework. Typical requests would be to create or delete clusters, merge multiple clusters, split clusters or associate tracks with clusters. This software engineering approach means that the framework can provide all memory-management and book-keeping operations in an efficient and well-tested manner.

4. Particle Flow Algorithms

The particle flow reconstruction at CLIC uses over 60 different PandoraPFA algorithms and tools. These algorithms are efficient and well-understood. The basic reconstruction operations performed by the default set of PandoraPFA algorithms can be summarised as follows:

- Calorimeter cells are clustered using a simple cone-based clustering algorithm. The algorithm works outwards from the innermost cells in the detector, either adding cells to existing clusters or seeding new clusters. Clusters can also be seeded by the projection of inner detector tracks to the front face of the calorimeter.
- The clustering algorithm is configured so as to split up the energy depositions from individual particles, rather than risk merging the depositions from multiple particles. The resulting cluster fragments are then carefully merged together by a series of algorithms that implement well-motivated topological rules.

- Calorimeter clusters are associated to inner detector tracks, by comparing the properties of the clusters (results of linear fits, helix fits, etc.) to the projected track positions and directions at the front face of the calorimeter.
- If the energy of a calorimeter cluster does not match the associated track momentum, the clustering can be reconfigured by the statistical reclustering algorithms. These use a series of differently configured clustering algorithms in order to investigate the possible cluster configurations achievable with the relevant cells and tracks. The cluster configuration offering the best track-cluster compatibility is selected.
- Fragment-removal algorithms aim to remove neutral clusters that are really fragments of charged clusters. The algorithms search for evidence of association between nearby clusters, whilst also considering the changes in track-cluster compatibility that would occur if the clusters were merged.
- Particle flow objects are formed. If a particle is composed of both tracks and clusters, its properties are extracted from measurements of the tracks. For neutral particles, calorimeter information is used.
- Particle identification algorithms are used throughout the reconstruction.

The original ideas for these algorithms are described in more detail in [2]. Since this publication, the algorithms have been re-examined and re-implemented using the PandoraPFA SDK. This new software implementation was used for all the physics performance studies presented in the CLIC conceptual design report [1]. It has been demonstrated [10] that the new implementation achieved identical physics performance, whilst offering sizeable reductions in memory usage and CPU-time requirements. The re-implementation also offered a number of software engineering improvements, ensuring that the code for each algorithm is simple, efficient and easy to maintain. Following the re-implementation of the original algorithms, further development focused on improving the reconstruction of high energy jets (above 250 GeV) in the presence of machine-induced background.

For very high energy jets, the energy deposits from particles within a jet inevitably overlap. In this case the pure pattern-recognition approach of particle flow reconstruction starts to break down. At this point, more emphasis is given to an energy flow approach, based

on the consistency of track momenta and associated calorimeter cluster energies. Improvements to the statistical reclustering algorithms ensure a smooth transition from pure particle flow to energy flow. These statistical reclustering algorithms can now be cleanly divided into the following categories:

- Algorithms that deal with multiple inner detector tracks associated to a single calorimeter cluster. These algorithms must try to split up the cluster.
- Algorithms that deal with clusters with energies significantly greater than the momentum of their associated inner detector tracks. These algorithms must also try to split up the clusters.
- Algorithms that deal with inner detector tracks with momentum significantly greater than the energy of their associated clusters. These algorithms must bring in nearby ‘neutral’ clusters and reconfigure the division of cells into clusters.

In order to ensure suitable track-cluster compatibility (an indication that confusion in the reconstruction is minimal), associated tracks and clusters must pass algorithms from each of the above categories without requiring modification. If changes are made, the new track-cluster configuration must also pass the full set of consistency checks. If, and only if, no consistent track-cluster configuration can be found, a ‘Forced Clustering’ algorithm is used to implement a transition to energy flow calorimetry. This algorithm selects calorimeter cells along a helix projection of the inner detector track until a new cluster with energy matching the track momentum is formed. The remnant hits are clustered independently and will typically form neutral particles. This managed transition to energy flow, which occurs only when algorithms cannot find a natural clustering configuration, proves to be important at high jet energies.

Further improvements for high energy reconstruction include new algorithms to identify MIP-like sections of calorimeter clusters and to track these sections through electromagnetic clusters in the ECAL. Improvements to the photon reconstruction have also been made, placing a series of careful selection cuts on ECAL clusters to ensure that the clusters match the expected longitudinal and transverse profiles for electromagnetic showers. Finally, particle identification functionality was added to tag photons and charged leptons. The particle identification information is actively used in the pattern-recognition reconstruction, aiding decisions when considering how to process certain clusters or reconstructed particles.

5. Background Considerations

The experimental environment at CLIC differs from that at previous e^+e^- colliders such as LEP:

- The high bunch-charge density, related to the small beam size at the interaction point, means that the electrons and positrons radiate strongly in the electromagnetic field of the other beam, an effect known as beamstrahlung.
- There are significant beam related backgrounds. The pile-up of approximately 3.2 multiperipheral $\gamma\gamma \rightarrow$ hadrons “mini-jet” events per bunch crossing is an important consideration in particle flow reconstruction at CLIC.
- The CLIC beam consists of bunch trains of 312 bunches with a train repetition rate of 50 Hz. Within a bunch train, the bunches are separated by 0.5 ns. The short time between bunches means that a detector will inevitably integrate over a number of bunch crossings.

If it is assumed that all detector systems integrate over 10 ns, the $\gamma\gamma \rightarrow$ hadrons background corresponds to 1.2 TeV of energy deposited in the calorimeter systems. This large background presents a challenge for particle flow reconstruction at CLIC. However, the combination of high granularity particle flow reconstruction and timing information can be used to greatly suppress this background.

5.1. Background suppression

The PandoraPFA algorithms aim to reconstruct the four-vectors of all visible particles in an event. A jet-finding algorithm can then be used to identify individual jets, with the jet energy reconstructed as the sum of the energies of the reconstructed particles (PFOs) in the jet. However, in the presence of beam-induced background, it is vital to identify and remove the background particles before the jet-finding stage. Based on full GEANT4 simulation studies, a realistic strategy for mitigating the effects of background was developed. This is based on the reconstructed p_T of the individual PFOs and timing information. In these studies a 1 ns timing resolution was assumed for hits in the calorimeters and all calorimeter and tracker hits within a 10 ns window, starting at the bunch crossing containing the physics event, were included in the reconstruction. Following the reconstruction of inner detector tracks, a CLIC-TRACKSELECTOR event processor was used to remove poor quality and fake tracks from events reconstructed

in the presence of background. This processor examines the number of track hits in each of the tracking sub-detectors and applies simple quality cuts. It also places a cut on the arrival time of the tracked particle at the front face of the calorimeter. Tracks are rejected if the arrival time, calculated using a helix fit to the track, differs by more than 50 ns from a simple straight-line time-of-flight calculation. The CLICTRACKSELECTOR is an important tool for background suppression and is used whenever background is added to an event and whenever any background suppression cuts are applied.

The main benefit of particle flow reconstruction is that it clusters the calorimetric energy in the detector into individual particles, which can then be identified as being from background or from the underlying hard interaction. Because hadronic showers take a finite time to develop, it is not possible to simply place very tight timing requirements on the individual hits prior to the reconstruction. Instead, the strategy is to perform particle flow reconstruction and then use the properties of the PFOs to either reject or retain the PFO. Each calorimeter cluster associated with a reconstructed PFO contains many individual hits. The hits are distributed in time due to the assumed time resolution and the development time of the shower. Furthermore, the clusters may contain hits from more than one particle; this is particularly important for the forward region, where the background from $\gamma\gamma \rightarrow$ hadrons is the greatest. For these reasons, timing cuts are applied at the cluster level using a robust mean of the individual hit times. The cluster time is calculated by first determining the median time of all hits in the cluster and then ignoring the times of the outlying 10% of hits. The times of the remaining hits are used to calculate an energy-weighted mean value, which is assigned to the cluster. If a cluster contains sufficient ECAL hits, only ECAL hits are considered in this calculation. With a single hit resolution of approximately 1 ns, mean cluster times with an accuracy much better than 1 ns are obtained.

The PFOs from the physics event have a range of p_T values and have times close to t_0 , where t_0 is the time of the bunch crossing containing the event; identified in the high-level software trigger. The PFOs from the $\gamma\gamma \rightarrow$ hadrons background tend to be at lower values of p_T and are distributed in time across the 10 ns reconstruction window. These two features allow background PFOs to be separated from signal PFOs. This is only made possible by the highly granular calorimeters. In a more conventional calorimeter, the energy deposits from signal and background would overlap. Figure 2 shows the p_T and time distributions for photon and neutral hadron PFOs in the endcap regions, for both signal

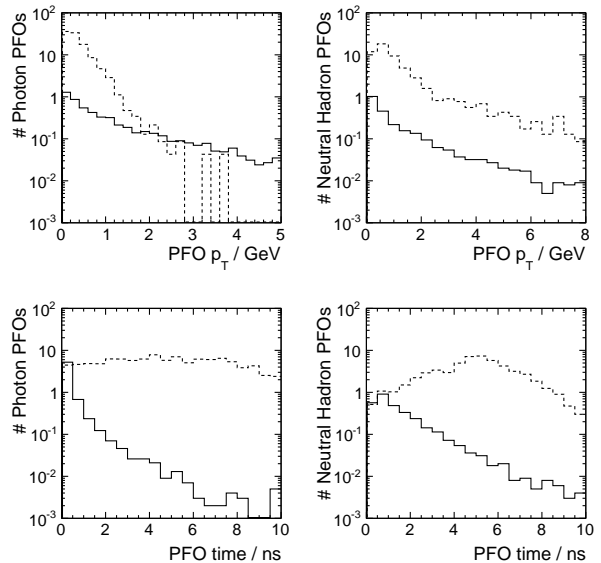


Figure 2: The PFO time and p_T distributions for reconstructed photon and neutral hadron PFOs. The solid histograms show the distributions for $ZZ \rightarrow \nu\nu q\bar{q}$ events at $\sqrt{s} = 3$ TeV and the dashed histograms show the distribution for pile-up from $\gamma\gamma \rightarrow$ hadrons.

and background. The two variables are largely independent. As expected, the time distribution for background photon PFOs is essentially flat. The reason that the background neutral hadron PFOs tend to peak at 5 ns is that the reconstructed clusters are often composed of energy deposits from multiple background particles, which is also reflected in the harder energy spectrum.

The optimal treatment of the background is likely to depend on the physics process being studied. For example, for final state processes which result in forward jets, harder timing cuts are likely to be beneficial. For this reason sets of background rejection cuts were developed. Cuts were only applied in the regions of p_T and time where there was a significant background component, $p_T < 4.0$ GeV for photon and charged PFOs and $p_T < 8.0$ GeV for neutral hadrons. Tighter cuts were applied in the far forward region, $|\cos\theta| > 0.975$, where background PFOs tend to be formed from energy deposits from multiple background particles. Tighter timing cuts were applied to PFOs with $p_T < 0.75$ GeV where there is a large contribution from background. The initial loose timing cuts, within the different p_T regions, were chosen to have minimal impact on PFOs from 500 GeV jets. Subsequently the cuts were optimised by modifying the timing cuts for each type of

PFO in steps of 0.5 ns. The final version of the CLIC-PFOSELECTOR algorithm has three available configurations, which apply `Default`, `Loose` and `Tight` cuts to the PFOs. The selection cuts for the `Loose` and `Tight` configurations are listed in Table 1. The `Tight` cuts also include the requirements that $p_T > 0.2 \text{ GeV}$ for photon PFOs and $p_T > 0.5 \text{ GeV}$ for neutral hadron PFOs; these additional cuts were found to be more effective than further tightening the timing cuts.

To illustrate the power of suppressing machine-induced background with the CLICPFOSELECTOR, Figure 3 shows the reconstructed particle flow objects for a simulated $e^+e^- \rightarrow H^+H^- \rightarrow t\bar{b}b\bar{t}$ event at $\sqrt{s} = 3 \text{ TeV}$. Assuming a time window of 10 ns for the silicon detectors, the ECAL and the HCAL endcap and 100 ns for the HCAL barrel, the background from $\gamma\gamma \rightarrow \text{hadrons}$ produces an average energy of approximately 1.2 TeV per event, mostly in the form of relatively low p_T particles at relatively low angles to the beam axis. As a result of the cluster-based `Tight` timing cuts, the average background level can be reduced to approximately 100 GeV with negligible impact on the underlying hard interaction. Table 2 summarises the impact of the different PFO selection cuts on the signal and background. The equivalent cut on p_T alone has a much larger impact on the signal than the combination of p_T and timing cuts.

Table 2: The impact of the different PFO selections on the reconstructed energy of $\gamma\gamma \rightarrow \text{hadrons}$, and of a hadronically decaying W boson of 500 GeV energy. The impact of a simple p_T cut is shown for comparison.

Cut	$\gamma\gamma \rightarrow \text{hadrons}$	500 GeV di-jet	
	Energy (GeV)	Energy (GeV)	Energy loss
No cut	1210	500.2	0%
Loose	235	498.8	0.3%
Default	175	498.0	0.5%
Tight	85	496.1	0.8%
$p_T > 3.0 \text{ GeV}$	160	454.2	9.2%

6. A Study of Particle Flow Performance

A study has been carried out to assess the performance of particle flow calorimetry at CLIC, and to investigate the variation of the performance with the jet energy, the angle and the PFO selection cuts. For this purpose, Z' particles were generated at energies ranging from 91 GeV to 3 TeV. These are off-shell Z bosons,

produced at rest at different centre-of-mass energies, which decay into light quarks and typically provide two back-to-back mono-energetic jets. For this initial study, no jet reconstruction was performed and backgrounds were not included; instead, to avoid bias, the full energy deposited in the detector, E_{jj} , was analysed. The performance of fully reconstructed physics observables in the presence of background is presented in Section 7.

The performance of the particle flow reconstruction was evaluated by calculating the resolution of the jet energy, E_j . This is defined as:

$$\frac{\text{RMS}_{90}(E_j)}{\text{mean}_{90}(E_j)} = \frac{\text{RMS}_{90}(E_{jj})}{\text{mean}_{90}(E_{jj})} \sqrt{2} \quad (1)$$

where the $\text{RMS}_{90}(E_{jj})$ and the $\text{mean}_{90}(E_{jj})$ are calculated from the total reconstructed energy distribution. The RMS_{90} is defined as the RMS in the smallest region of reconstructed energy that contains 90% of the events. It is introduced in order to reduce sensitivity to tails in a well defined manner, because the effects of confusion mean that the PFO energy distribution will be inherently non-Gaussian [2].

6.1. Jet Energy Resolution

As the jet energy increases, the jets become narrower and it becomes more difficult to distinguish individual particles. Particle flow calorimetry can turn into energy flow calorimetry and the effects of confusion will dominate the jet energy resolution. Figure 4 shows the distribution of the reconstructed jet energy for a number of different jet energies. The Figure also shows the variation of the jet energy resolution as a function of the jet energy for jets in the barrel region of the detector, defined by $|\cos(\theta)| < 0.7$, where θ is the polar angle of the generated quarks. Compared to previous results obtained in [2], significant improvements to the jet energy resolution have been achieved with the new PandoraPFA algorithms. The improvements are particularly noticeable at high jet energies; the jet energy resolution is better than 3.7% over the range of jet energies considered. Whilst the results presented here are for the barrel region of the detector, a jet energy resolution of 4% or better is achieved in the endcap region, only worsening slightly at $0.95 < |\cos \theta| < 0.975$, corresponding to angles as small as 12.8° . The full variation of the jet energy resolution with polar angle is shown for both CLIC detector concepts in [1].

6.2. PFO Selection Cuts

In order to assess the impact of the CLICPFOSELECTOR on underlying physics events, the $Z' \rightarrow q\bar{q}$ events

Table 1: Cuts applied by the CLICPFOSELECTOR in the Loose and Tight configuration modes.

	Loose configuration		Tight configuration	
Region	p_T range [GeV]	Time [ns]	p_T range [GeV]	Time [ns]
Photons				
Central	$0.75 \leq p_T < 4.0$	$t < 2.0$	$1.0 \leq p_T < 4.0$	$t < 2.0$
$ \cos(\theta) \leq 0.975$	$0 \leq p_T < 0.75$	$t < 2.0$	$0.2 \leq p_T < 1.0$	$t < 1.0$
Forward	$0.75 \leq p_T < 4.0$	$t < 2.0$	$1.0 \leq p_T < 4.0$	$t < 2.0$
$ \cos(\theta) > 0.975$	$0 \leq p_T < 0.75$	$t < 1.0$	$0.2 \leq p_T < 1.0$	$t < 1.0$
Neutral hadrons				
Central	$0.75 \leq p_T < 8.0$	$t < 2.5$	$1.0 \leq p_T < 8.0$	$t < 2.5$
$ \cos(\theta) \leq 0.975$	$0 \leq p_T < 0.75$	$t < 1.5$	$0.5 \leq p_T < 1.0$	$t < 1.5$
Forward	$0.75 \leq p_T < 8.0$	$t < 2.5$	$1.0 \leq p_T < 8.0$	$t < 1.5$
$ \cos(\theta) > 0.975$	$0 \leq p_T < 0.75$	$t < 1.5$	$0.5 \leq p_T < 1.0$	$t < 1.0$
Charged particles				
All	$0.75 \leq p_T < 4.0$	$t < 3.0$	$1.0 \leq p_T < 4.0$	$t < 2.0$
	$0 \leq p_T < 0.75$	$t < 1.5$	$0 \leq p_T < 1.0$	$t < 1.0$

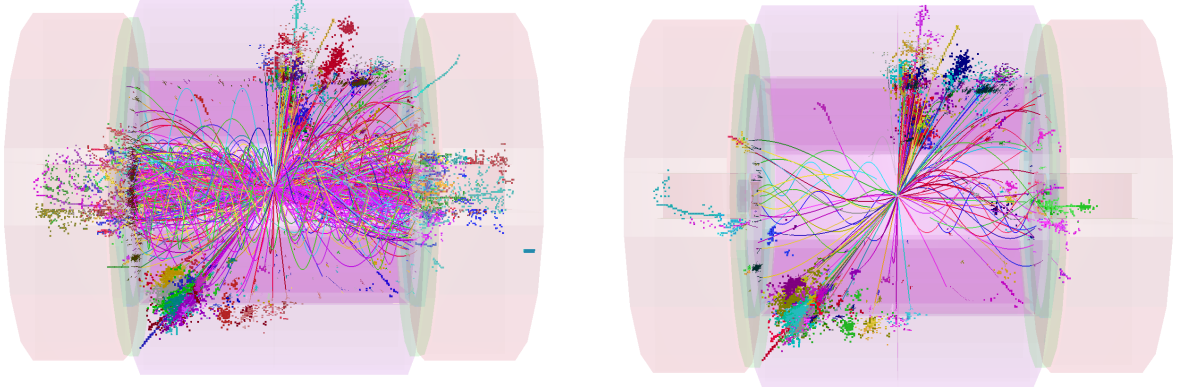


Figure 3: Reconstructed particles for a time window of 10 ns (100 ns in HCAL barrel) in a simulated $e^+e^- \rightarrow H^+H^- \rightarrow t\bar{b}b\bar{t}$ event in the CLIC.ILD detector, with 60 BX of $\gamma\gamma \rightarrow$ hadrons background overlaid (left). The effect of applying Tight PFO selection cuts to the reconstructed particles is shown on the right; the energy deposited in the detector by the background is reduced from 1.2 TeV to the level of 100 GeV.

described in Section 6 were used again. Without any backgrounds, the Z' events were examined after the application of the different PFO selection cuts. Figure 5 shows the sum of the reconstructed PFO energies for 91 GeV Z' events, before application of PFO selection cuts. Separate distributions are shown after application of the Loose and Tight cuts described in Table 1. The more stringent the cuts, the more energy is cut

away. Equivalent distributions are also shown for 1 TeV $Z' \rightarrow q\bar{q}$ events, indicating that any negative impact of the PFO selection cuts decreases with energy.

Figure 6 illustrates the impact of the CLICPFOSELECTOR on the jet energy resolution as a function of the jet energy. At low jet energies, the PFO selection cuts have a significant impact on the jet energy resolution. As the jet energy increases, the jet energy recon-

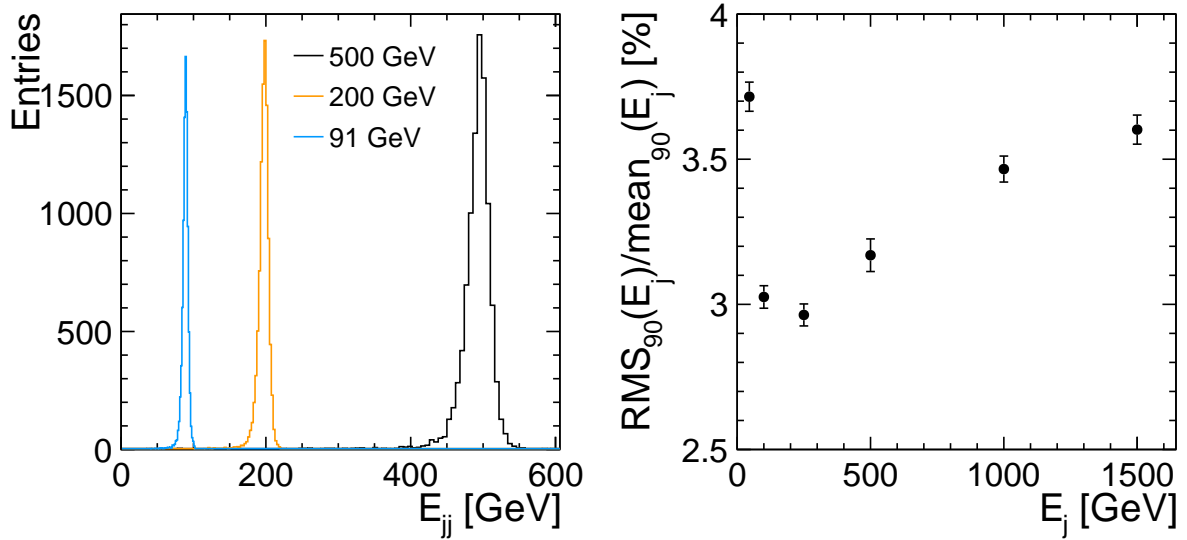


Figure 4: The total reconstructed energy for three centre-of-mass energies (left) and the jet energy resolution as function of the jet energy (right) for jets from simulated $Z' \rightarrow q\bar{q}$ decays. The jet energy resolutions represent only jets in the barrel region of the detector.

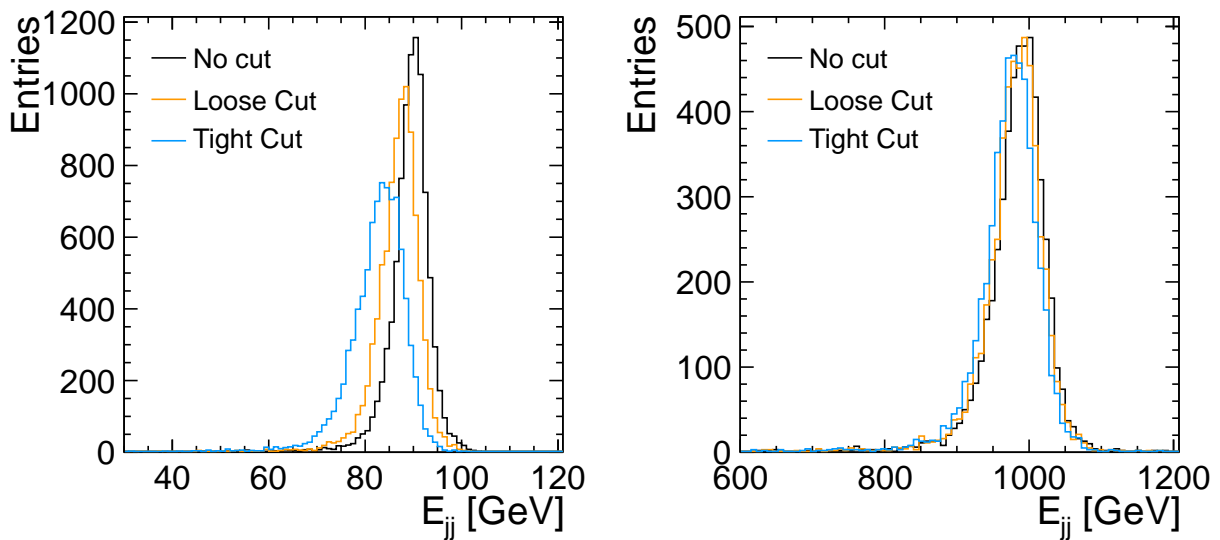


Figure 5: The impact of the the PFO selection cuts on the total reconstructed energy at $\sqrt{s} = 91$ GeV (left) and $\sqrt{s} = 1$ TeV (right), for jets from simulated $Z' \rightarrow q\bar{q}$ decays.

struction performance becomes the same with or without application of the PFO selection cuts.

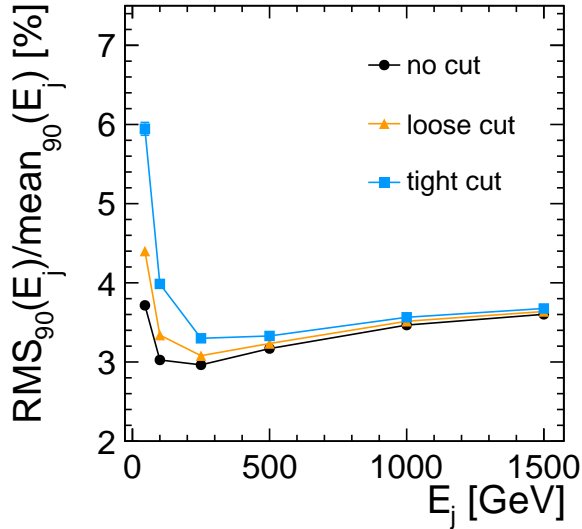


Figure 6: The impact of PFO selection cuts on jet energy resolution for jets from simulated $Z' \rightarrow q\bar{q}$ decays.

7. Particle Flow Physics Performance

7.1. W and Z Reconstruction

In order to study the physics performance achievable using particle flow calorimetry at CLIC, the ability to distinguish between W and Z particles was examined. The W events used for this study each contain two W bosons, one of which decays into a muon and neutrino, whilst the other decays into quarks. Events were generated for W energies of 125, 250, 500 and 1000 GeV. The main background for physics at CLIC is from the $\gamma\gamma \rightarrow$ hadrons mini-jet events. For each bunch crossing (BX), a number of $\gamma\gamma \rightarrow$ hadrons events was superimposed on the physics event; the number of events to be overlaid in this way was drawn from a Poisson distribution, assuming a mean of 3.2 events per BX [11]. For each W energy, samples were produced without background (0 BX) and with background overlaid to represent sixty bunch crossings (60 BX). To further study the impact of background on physics performance, additional samples were produced with a safety factor of two in the background estimation, corresponding to a mean of 6.4 $\gamma\gamma \rightarrow$ hadrons per BX.

All samples were fully simulated and reconstructed. Additional reconstruction and event selection procedures were then applied as described below:

- **Lepton Removal:**
The muon and every particle around it within a

cone of $|\cos\alpha| > 0.9$ was removed, leaving only the hadronic decay of one W in the event.

- **Removal of Neutral Fragments:**
If background had been overlaid, low energy neutral fragments in the forward region ($|\cos\theta| > 0.9$) were carefully removed. Fake neutral PFOs are likely to be created in this region due to unsuccessful matches between low p_T curling tracks and associated calorimeter clusters. A minimum energy threshold was applied for neutral PFOs in the region, with a cut ranging between 1 and 8 GeV, depending on the centre-of-mass energy.
- **Jet Reconstruction:**
Following evaluation of a number of jet reconstruction algorithms, the FastJet library [12] was selected and the kt algorithm used in exclusive mode to force the event into two jets. A scan of the R parameter for the jet cone size was performed at each energy, with and without background, and for each set of CLICPFOSELECTOR cuts: Default, Loose and Tight. No significant differences were observed for the different PFO selections. The best R values were found to be 0.7 with background and 1.5 without background.

The performance of particle flow calorimetry is closely linked to the quality of the jet reconstruction. Use of a single jet reconstruction algorithm for all configurations is not optimal, but does simplify the comparison of events with and without background. For this reason, the same jet reconstruction was chosen for use with all samples.

- **Event Selection:**
Both jets were required to have $|\cos\theta| < 0.9$, to stay well within the detector acceptance. In addition, a lower limit on the angle between the two jets was applied, to reject events where the jet reconstruction failed. The lower limit depended on the energy of the W and was based on the expected range of angles for the generated events.

The need for the PFO selection cuts in the presence of background is clearly illustrated in Figure 7, which shows the reconstructed energy and mass distributions for the 500 GeV W samples. Separate distributions are shown for the samples without background, and the 60 BX sample with and without PFO selection cuts. Without the application of the PFO selection cuts, many background particles remain in the event and are reconstructed as part of the jet. These particles shift the jet energy distribution to higher values and tend to

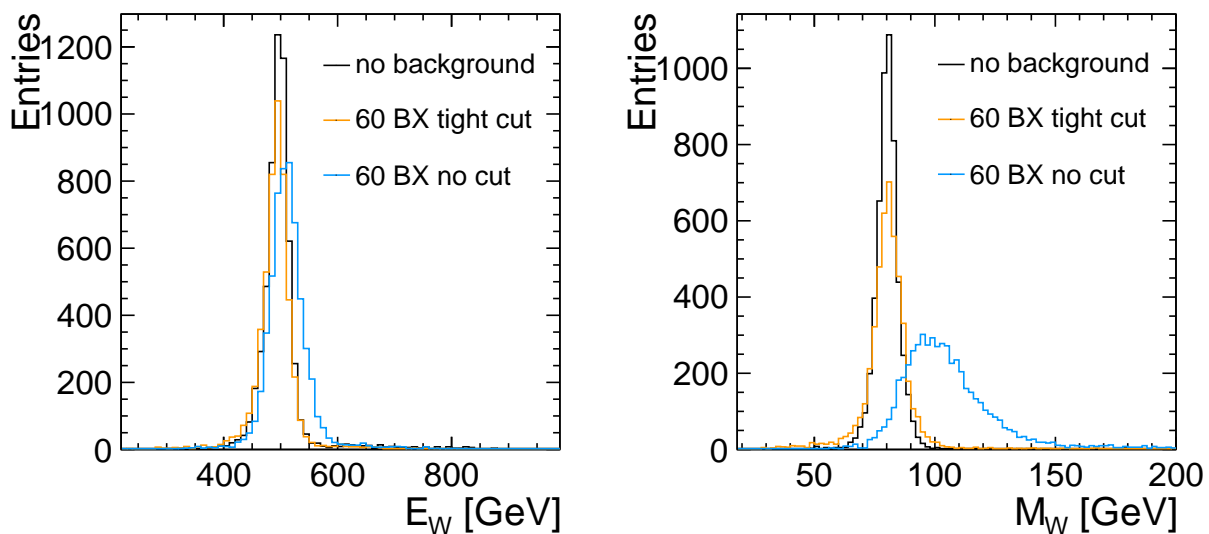


Figure 7: Energy (left) and mass (right) distributions of reconstructed W at an energy of 500 GeV. Separate distributions are shown for events without background and for events with 60 BX of background before and after application of Tight PFO selection cuts.

bias the reconstructed jet axis towards the beam axis. Consequently, the reconstructed di-jet mass distribution is badly distorted. With the PFO selection, a narrow W mass peak is recovered. It is found that the differences between the three PFO selection cuts are small and henceforth only the Tight cuts are considered.

The energy and mass resolutions were studied by calculating the RMS_{90} and mean_{90} for the distributions of jet energy and jet mass. With the overlay of 60 BX of background, the energy and mass distributions were distorted and the tails became more prominent. The RMS_{90} method to calculate the resolution is robust against these changes, whilst considering all features of the distribution, not just the main part of the peak. The resolutions given in this section are therefore purely a measure of peak quality, but cannot be used directly to assess the power to distinguish between W and Z particles. This is addressed in Section 7.2.

Figure 8 shows the energy and mass resolution of the reconstructed W as a function of the W energy. Separate distributions are shown for the samples without background, for the samples with 60 BX of background and for the samples with 2×60 BX of background. Without background, the resolutions are comparable to those obtained in the study described in Section 6, without jet reconstruction. In the presence of background, the degradation of the energy resolution at lower energies

is significant. With increasing W energy, the impact of the background on the energy resolution becomes rather small. As the mass resolution is more sensitive to the jet quality, the background still leads to appreciable degradation of the mass resolution, even at higher energies. The additional degradation upon moving from 60 BX to 2×60 BX of background is rather small.

7.2. W and Z Separation

A key requirement for the physics programme at CLIC is the ability to separate hadronic W and Z decays. For this purpose, the di-jet mass distributions obtained from the simulated W decays were compared to those obtained from Z decays using simulated $e^+e^- \rightarrow ZZ \rightarrow \nu\bar{\nu}q\bar{q}$ events. As for the W datasets, fully simulated and reconstructed events were available with Z energies of 125, 250, 500 and 1000 GeV. Samples were produced without background and with 60 BX and 2×60 BX of overlaid $\gamma\gamma \rightarrow \text{hadrons}$ background. The same reconstruction and selection procedure was used and the reconstruction performance was found to be very similar to that obtained for the Ws. Figure 9 shows the reconstructed mass peaks for W and Z particles with an energy of 500 GeV. Without background, there is clear separation between the peaks. With 60 BX of background, the separation is somewhat degraded.

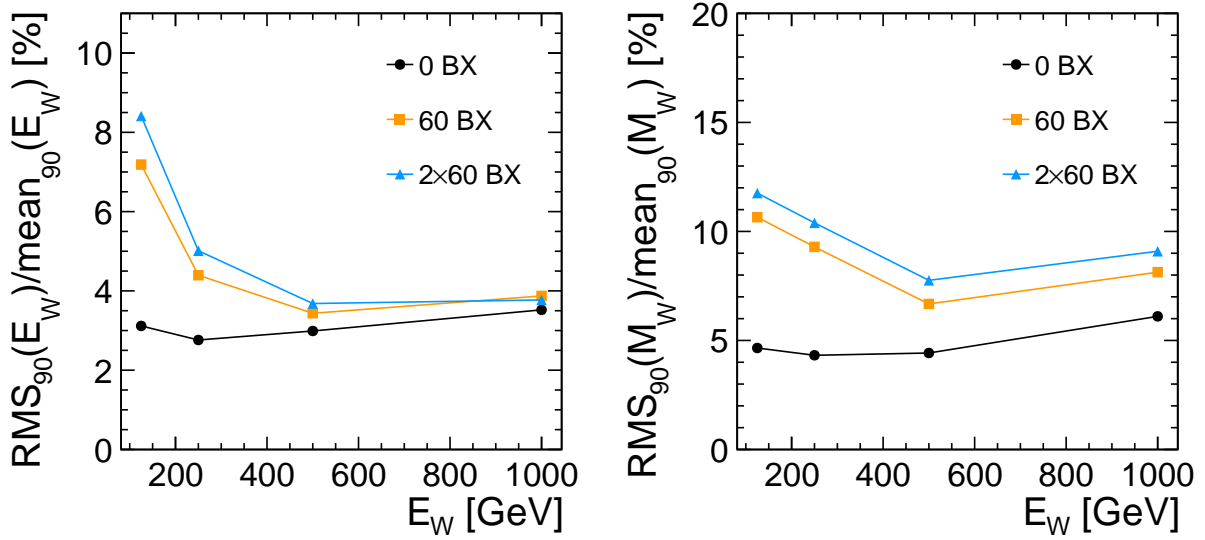


Figure 8: Energy (left) and mass (right) resolutions of reconstructed W, for events without background and for events with 60 BX and 2×60 BX of background. Tight PFO selection cuts are used for events with background.

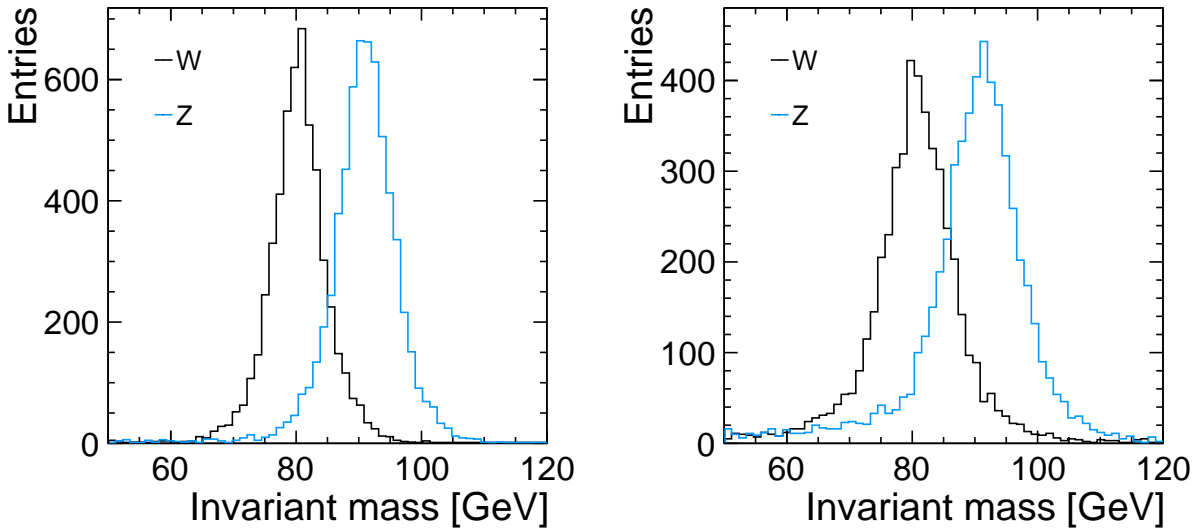


Figure 9: Mass distributions of reconstructed W and Z at an energy of 500 GeV, without background (left) and with 60 BX of background (right). Without background the separation is 2.2σ . With 60 BX of background the separation drops to 1.8σ . Tight PFO selection cuts are used for events with background.

Table 3 summarises the mass resolutions obtained for the W and Z samples and the separation achieved and the identification efficiency for each of the different energies investigated. The separation of the W and Z

peaks is quantified by determining the fraction of misidentified events for the optimum mass cut. The natural widths of the W and Z bosons restrict the identification efficiency to $< 94\%$ [2]. The fraction of mis-

Table 3: Mass resolutions obtained for reconstructed W and Z at different energies and with different amounts of overlaid background. The separation of the W and Z peaks and the identification efficiencies are labelled for each configuration. Tight PFO selection cuts are used for events with background.

BX	$E_{W,Z}$ [GeV]	$\sigma_{m(W)}/m(W)$ [%]	$\sigma_{m(Z)}/m(Z)$ [%]	Separation [σ]	ϵ [%]
0 BX	125	4.6	4.2	2.2	88
	250	4.3	4.0	2.2	89
	500	4.4	4.2	2.2	88
	1000	6.1	5.4	1.9	87
60 BX	125	10.7	10.1	1.5	70
	250	9.3	9.0	1.6	74
	500	6.7	6.6	1.8	79
	1000	8.1	7.7	1.7	77
2 \times 60 BX	125	11.8	11.0	1.4	67
	250	10.4	10.2	1.5	71
	500	7.8	7.9	1.6	74
	1000	9.1	8.5	1.6	73

identified events is converted into an equivalent Gaussian statistical separation, where for example, in the case of ideal Gaussian distributions, a mis-identification of 15.8% corresponds to a separation of 2σ . Without background a 2σ separation of the W and Z mass peaks is essentially maintained for gauge bosons with energies between 125 GeV and 1 TeV. This separation is reduced to about 1.7σ when background is included. Even without the background, it would be exceedingly difficult to achieve such a level of separation (over such a wide range of jet energies) using a traditional approach to calorimetry. The successful use of particle flow calorimetry to separate hadronic W and Z decays in a physics analysis is demonstrated in [1].

7.3. Measurement of Missing Momentum

The reconstruction of missing momentum is important in many physics processes. Here, the performance of the particle flow reconstruction of missing momentum is quantified in two ways: i) the missing momentum resolution for events with a true missing momentum signature; and ii) the reconstructed missing momentum in event topologies where the momentum of the reconstructed particles should balance.

Resolution of Missing Transverse Momentum

The missing transverse momentum resolution was quantified using the simulated $ZZ \rightarrow \nu\bar{\nu}q\bar{q}$ events discussed in Section 7.1. The jet reconstruction was un-

changed, and the only event selection requirement was that both jets satisfy $|\cos\theta| < 0.9$. The missing momentum depends on both the energies of the neutrinos and their polar angles. For this reason the four different energy points, $\sqrt{s}=250, 500, 1000$ and 2000 GeV, were combined into a single data set. The missing transverse momentum, \cancel{p}_T , was calculated from the vector sum of the momenta of all the particles in the two reconstructed jets. This was compared to the generated missing transverse momentum of the two neutrinos, $\cancel{p}_{T,true}$. Figure 10 shows the distribution of the difference between measured and true missing transverse momentum (for all events combined) and the missing transverse momentum resolution as a function of the true p_T in the event. For each bin in p_T , the missing transverse energy resolution was obtained by calculating the RMS_{90} of the $\Delta\cancel{p}_T$ distribution and dividing by the true missing transverse momentum. The resolutions obtained indicate that the missing transverse momentum can be measured with an asymptotic precision of about 3% for $p_T > 100$ GeV.

Fake Missing Momentum

Many physics analyses rely on measurements of missing momentum. Fake missing momentum can result from limitations in the detector coverage and from the mis-reconstruction of the momenta of the particles. The fake missing momentum was quantified using the $Z' \rightarrow q\bar{q}$ events described in Section 6. The events were reconstructed into three jets, to account for the possibil-

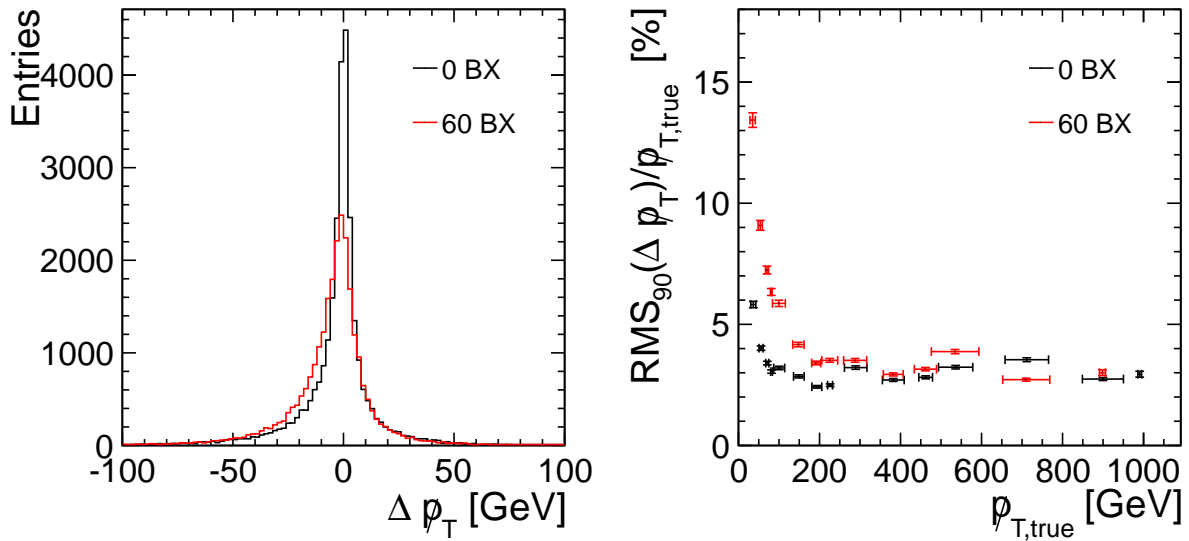


Figure 10: Distribution of the difference between measured and true missing transverse momentum (left) and the missing transverse momentum resolution (right) for $ZZ \rightarrow \nu\bar{\nu}q\bar{q}$ events. Separate distributions are shown for events without background and with 60 BX of background. Tight PFO selection cuts are used for events with background.

ity of a single hard gluon radiation. Figure 11 shows the distribution of the x component of the fake missing momentum for the 91 GeV Z' sample. The resolution was quantified by calculating the RMS_{90} of this distribution. The right hand plot of Figure 11 shows that the RMS_{90} rises approximately linearly with the total energy deposited in the detector. Overall, the level of fake missing transverse momentum (in one coordinate) is at the level of 1-2% of the event energy. The impact of the $\gamma\gamma \rightarrow \text{hadrons}$ background is not large for the event energies of interest at CLIC.

8. Summary

Particle flow calorimetry is an extremely powerful technique, which can deliver unprecedented energy and mass resolutions at future linear colliders, even in the challenging environment at CLIC. The PandoraPFA particle flow algorithm now offers an accurate particle flow reconstruction at jet energies from 50 GeV to 1.5 TeV, and includes a managed transition to energy flow calorimetry if calorimeter occupancies become exceptionally high. Following the particle flow reconstruction, timing cuts can be applied to reconstructed particles to significantly reduce the contribution of beam-induced backgrounds.

The energy dependence of the particle flow reconstruction, and the systematic effects of detector acceptance, have been investigated via a study of monoenergetic jets with energies up to 1.5 TeV. Two physics channels, providing W and Z particles, were then chosen to study the performance of particle flow calorimetry with jet reconstruction and in the presence of background. The energy and mass resolutions achieved are very promising. At higher energies, the effect of the $\gamma\gamma \rightarrow \text{hadrons}$ background on the energy resolution is negligible. The mass resolution is more sensitive to the quality of the reconstructed jets, and so is more strongly affected by backgrounds, but the separation of hadronic W and Z decays remains achievable. Even though PandoraPFA is not optimised for the reconstruction of missing momentum, it allows missing transverse momentum to be measured with the same precision as jet energies. The level of fake missing transverse momentum (in one coordinate) is at the level of 1-2% of the event energy.

Compared to previous results, obtained in [2], significant performance improvements have been achieved with the PandoraPFA algorithms, especially for higher jet energies. These improvements are evident in the jet energy resolution and in the ability to distinguish between the hadronic decays of W and Z particles. The PandoraPFA reconstruction has been used for all the simulated physics studies presented in the CLIC Con-

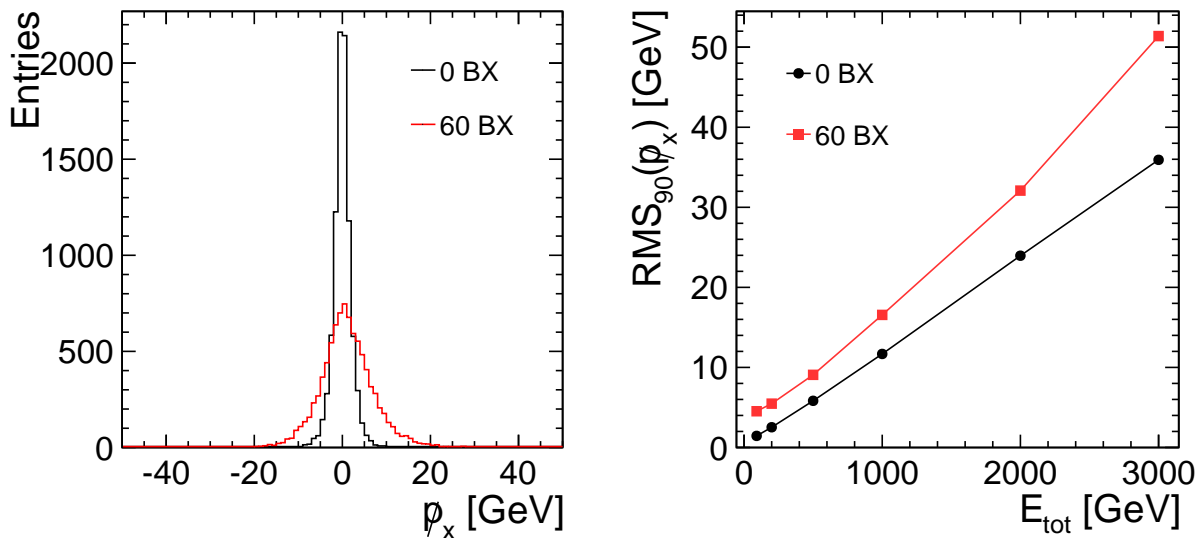


Figure 11: The x component of fake missing momentum for Z' events at 91 GeV (left) and the RMS_{90} of this distribution as a function of the total energy deposited in the detector (right). Separate distributions are shown for events without background and with 60 BX of background. Tight PFO selection cuts are used for events with background.

ceptual Design Report [1].

Acknowledgements

This work was funded in part by the UK Science and Technology and Facilities Council and by the European Union under the Advanced European Infrastructures for Detectors and Accelerators (AIDA) project.

References

- [1] L. Linssen et al., *Physics and Detectors at CLIC: CLIC Conceptual Design Report*, CERN-2012-03, 2012.
- [2] M.A. Thomson, *Particle Flow Calorimetry and the PandoraPFA Algorithm*, Nucl. Instr. and Meth. A 611 (2009) 25.
- [3] A. Münnich and A. Sailer, *The CLIC ILD CDR Geometry for the CDR Monte Carlo Mass Production*, LCD-Note-2011-002, 2011.
- [4] C. Grefe and A. Münnich, *The CLIC SiD.CDR Detector Model for the CLIC CDR Monte Carlo Mass Production*, LCD-Note-2011-009, 2011.
- [5] J. S. Marshall, A. Münnich, M. A. Thomson *Particle Flow Performance at CLIC*, LCD-Note-2011-028, 2011.
- [6] I.G. Knowles and G.D. Lafferty, *Hadronization in Z^0 decay*, J. Phys. G 23 (1997) 731.
- [7] M.G. Green, S.L. Lloyd, P.N. Ratoff, D.R. Ward, *Electron-Positron Physics at the Z*, IoP Publishing, 1998.
- [8] ALEPH Collaboration, D. Buskulic et al., *Performance of the ALEPH detector at LEP*, Nucl. Instr. and Meth. A 360 (1995) 481.
- [9] CMS Collaboration, *CMS Physics Analysis Summary*, CMS-PAS-PFT-09-001, 2009.
- [10] J.S. Marshall, *Redesign of PandoraPFA*, Report at IWLC 2010, October 19, 2010, Geneva.
- [11] P. Schade and A. Lucaci-Timoce, *Description of the signal and background event mixing as implemented in the Marlin processor OverlayTiming*, LCD-Note-2011-006, 2011.
- [12] M. Cacciari and G.P. Salam, *Dispelling the N^3 myth for the k_t jet-finder*, Phys. Lett. B 641 (2006) 57.